Int. J. Electrochem. Sci., 13 **(2018)** 10233 – 10246, doi: 10.20964/2018.11.70

International Journal of
ELECTROCHEMICAL
SCIENCE
www.electrochemsci.org

Synthesis, Thermal Stability and Electrocatalytic Activities of *meso*-tetrakis (5-bromothiophen-2-yl) Porphyrin and Its Cobalt and Copper Complexes

I. Elghamry[1,*], *S. S. Ibrahim*[2], *M. Abdelsalam*[1], *Y. Al-Faiyz*[1], *M. Al-Qadri*[1]

[1] Department of Chemistry, King Faisal University, P. O. Box 380 Al-Hofuf, 31982 Al-Ahsa, Saudi Arabia.
[2] Department of Physics, King Faisal University, P. O. Box 380 Al-Hofuf, 31982 Al-Ahsa, Saudi Arabia.
[*]E-mail: ielghamry@kfu.edu.sa, elghamry@hotmail.com

Received: 11 July 2018 / *Accepted:* 12 September 2018 / *Published:* 1 October 2018

Linearly *pi*-extended thienyl porphyrin namely 5,10,15,20 tetrakis (5-bromothiophen-2-yl) porphyrin, and its cobalt and copper complexes were synthesized in good and quantitative yields respectively. The chemical structure of the synthesized porphyrins was confirmed by spectroscopic techniques (FT-IR, NMR, MS, and UV-Vis). Additionally, the thermal gravimetric analysis (TGA) was measured to investigate the high-temperature stability of the porphyrins. Subsequently, the porphyrins were used as electrocatalysts for the oxygen evolution reaction (OER) in 1 M KOH. The cobalt-porphyrin complex showed the best performance in term of a low band gap value and a high catalytic activity with good stability towards the OER.

Keywords: Metalloporphyrin; Thermal stability; Electrocatalytic activity; Oxygen evolution reaction.

1. INTRODUCTION

A plethora of porphyrin macromolecule has been the active core of many studies in the last decades [1-3]. The high interest in the porphyrin is due to the exceptional chemical skeleton with characterized absorption in both UV-Vis and NIR regions [4,5]. Additionally, some of the porphyrin derivatives like metalloporphyrins have proven to possess robust thermal stability and oxidative decomposition properties compared to other organometallic compounds [6-8]. Therefore, organic materials with porphyrin scaffold in their chemical structure have played a significant role in many applications. For example, it is used in medicine for treating cancer in photodynamic therapy (PDT) and other diseases [9,10] liquid crystal and memory storage arrays technology [11-13], catalysis for

water splitting and renewable energy generation [14-20], molecular recognition sensors in different fields [21-29], and as dyes for sensitized solar cells (DSSC's) [30,31]. Particular applications, like catalysis process and sensitizing solar cells often take place at extremely high temperatures, therefore required materials with good thermal stability and high electric conductivity [324-34]. Since the lead report of Alder *et al*. in 1967 [35], which described that, *meso*-tetraphenylporphyrins (TPP) are thermally stable and sublime at a temperature above 350 ^{o}C, most of the thermal stability reports on the tetraarylporphyrins (TAP) are focused on the tetraphenyl derivatives [36-38]. An incisive survey on literature, it was noticed that reports on the thermal stability of the hetroarylporphyrins (HAP) with one or more heterocyclic ring, e.g. thiophene, at *meso*- positions of the porphyrin ring are extremely scarce [39]. Furthermore, thiophene heterocyclic ring systems are extensively used in engineering polyconductive polymers (PC) with unique semiconducting and electric characters [40-41]. Therefore, inserting thiophenes into a porphyrin scaffold at *meso*-position(s) will extend the *pi*-electron system of the porphyrin moiety, and in turn, would enhance its electric conductivity and structural stability.

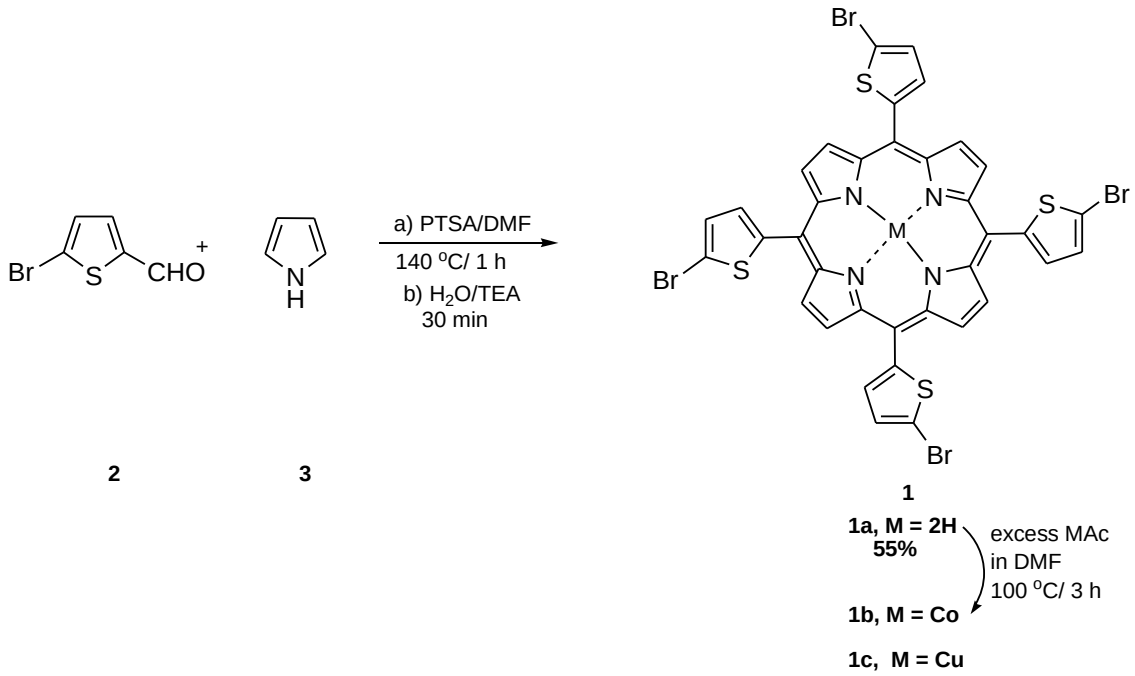

Scheme 1. Synthesis of 5,10,15,20-tetra(5-bromothiophen-2-yl) porphyrin and its cobalt and copper complexes (1a, 1b and 1c respectively)

Porphyrins possess high electric conductivity were used as a catalyst for several reactions, e.g., hydrogen evolution reactions (HER) [42, 43]. Bocarsly *et al*. [44] modified the surface of the glassy carbon electrode with cobalt porphyrin by oxidative electropolymerization. Then, the modified electrode was used to catalyze the reduction of CO_2 to CO. On the other hand, only few examples in the literature reported the use of metalloporphyrins as oxygen evolution catalysts. Du *et al*. [45] have reported water insoluble cobalt porphyrin complexes to fabricate films on the electrode and used it as a catalyst for water oxidation.

Herein, we report a comprehensive study on one of the *meso*-HAPs namely 10,15,20 tetrakis(5-bromothiophen-2-yl) porphyrin and its cobalt and copper complexes. This work covers the synthesis of the targeted porphyrins with a modified literature procedure (scheme 1). The UV-Vis absorption spectra, ^{1}H-NMR and FTIR techniques were used to confirm the structure of the synthesized materials. Also, band gap values were calculated. Thermal stability was investigated. Then, the electrocatalytic activities of Pt electrodes coated with the target porphyrin towards oxygen evolution reaction (OER) were examined.

2. EXPERIMENTAL

2.1 Materials and Methods

All solvents and starting materials were purchased from Sigma Aldrich and used directly without any further purification unless otherwise mentioned. The ultraviolet-visible (UV-Vis) spectra were acquired on GENESYS 10S UV-VIS Spectrophotometer. Infrared (IR) spectra were recorded using an Agilent Technologies Cary 630 FTIR spectrometer. The NMR spectra were measured with BRUKER Nuclear Magnatec Resonance 850 MHT spectrometer in $CDCl_3$. EI-MS spectra were recorded on Shimadzu QP-2010 PULS spectrometer. Chromatographic separations were performed using columns with silica gel (400 A^o) mesh. The thermal gravimetric analyses (TGA) were performed for 10 mg of a porphyrin sample using the TGA instrument (TA Instruments - Q50), under nitrogen atmosphere with a heating rate of 10 °C/min, from 25 to 700 °C. Samples were thoroughly dried in a Buchi glass oven B-585 at 100 °C under vacuum for 10 hours before performing the TGA analysis.

2.2 Synthesis of 5,10,15,20- tetrakis(5-bromothiophen-2-yl) porphyrin **(1a).**

A mixture of pyrrole (**3**) (1 ml, 14.9 mmol), and 5-bromothiophene-2-carbaldehyde (**2**) (1.8 ml, 14.8 mmol) in dimethylformamide DMF (10 ml) was heated at 100 ^{o}C under argon atmosphere. Then, *p*-toluenesulfonic acid (PTSA) (2.82 g, 16.37 mmol) was added, the reaction mixture was heated up gradually to 140 ^{o}C and kept at this temperature for one hour. The obtained dark violet solution was left to cool to room temperature. Then, poured into a mixture of cooled water and triethylamine (H_2O/TEA 95: 5 v/v) and left for 30 min. with stirring. The solid precipitate was filtered, washed several times with water, air dried and purified by column chromatography ($CHCl_3$/MeOH 99:1 v/v) and crystallized from $CHCl_3$/MeOH.

The free base porphyrin (**1a**) was obtained as dark purple crystals in 55% yield (1.77 g), m.p. over 250 ^{o}C. FT-IR (cm^{-1}): 3415, 1598, and 950 (the in-phase stretching, in-plane deformation and the out-plane deformation vibration modes of the N-H bonds, respectively) 3110 (C-H aromatic stretching vibration). ^{1}H-NMR ($CDCl_3$): δ in ppm : 9.23 (8 β– hydrogens of the porphyrin ring), 7.42 (m, H-4 of the thiophene rings), 6.56 (m, H-3 of the thiophene rings), -2.52 (2H-,inner NH of the porphyrin ring). Ms**;** (m/z) for $C_{36}H_{18}Br_4N_4S_4$ M.wt 954 (M^+), 955 (M^{+1}) ,638 (100%). UV–Vis (CH_2Cl_2**)**, λ_{max} (nm): 432 nm (soret bands), 523 nm, 563 nm, 596 nm, 655 nm (Q bands)

2.3 Synthesis of metalloporphyrins **(1b, c**)

A mixture of porphyrin (**1a**) (100 mg, 0.09 mmol) and metal acetate (0.3 mmol) was dissolved in DMF (5 ml). The reaction mixture was heated-up and kept at 100 ^{o}C under argon atmosphere for 3 hours, left to cool then poured into cooled water. The solid product was collected by filtration, washed by water several times, air dried, purified by column chromatography ($CHCl_3$/MeOH 99:1 v/v) and crystallized from $CHCl_3$/MeOH.

2.3.1 5,10,15,20-tetrakis(5-bromothiophen-2yi)porphyrinato cobalt (II) (**1b**)

It was obtained as dark violet crystals with almost quantitative yield and crystallized from $CHCl_3$/MeOH, m. p. over 250 ^{o}C. ^{1}H-NMR ($CDCl_3$): δ = 7.44-8.41 ppm (m, Ar-H). ^{13}C-NMR ($CDCl_3$): δ = 115.1, 116.2, 119.8,122.5, 125.3, 128.6, 131.5, 135.2, 139.2, 140.6, 158.7, 164.5. Ms (EI): (m/z):1009, 1010, 1014 (M^+) (M+1, M+2) for $C_{36}H_{16}Br_4CoN_4S_4$. UV–Vis (CH_2Cl_2), λ_{max} (nm): 419 nm (soret bands), 537 nm (Q bands)

2.3.2 5,10,15,20-tetrakis(5-bromothiophen-2yi)porphyrinato copper (II) (**1c**)

It was obtained as dark violet crystals with almost quantitative yield and crystallized from $CHCl_3$/MeOH, m.p. over 250 ^{o}C. ^{1}H-NMR ($CDCl_3$): δ = 7.26- 8.17 ppm (m, Ar-H). Ms (EI): (m/z) for $C_{36}H_{16}Br_4CuN_4S_4$, 1015 (M^+), 1016 (M+1), 1017 (M+2), 1018 (M+3). UV–Vis ($CHCl_3$), λ_{max} (nm): 430 nm (soret bands), 548 nm (Q bands).

2.4 Preparation of electrocatalyst electrodes and electrochemical measurements.

A platinum electrode of 1 mm diameter was used as a base electrode. Porphyrin electrocatalyst was prepared by coating the platinum electrode with a layer of the targeted porphyrin (the free base porphyrin **1a**, cobalt-porphyrin **1b** or copper-porphyrin **1c**). The coating process was performed by forming a slurry of 10 mg of porphyrin in 100-µl dichloromethane using the ultrasonic bath for 30 min. Then, 10 µl of the obtained slurry was deposited on the top of the platinum electrode. Subsequently, the electrode was dried at 50 °C for 10 minutes. The coating process was repeated until the electrode was fully loaded with the 10 mg of porphyrin. The deposited layer was very stable and adhered very well to the surface of the platinum electrode.

Electrochemical measurements were performed using EZstat potentiostat/galvanostat supported with EZware software. The measurements were carried out in a conventional three-electrode cell. The coated Pt electrode was used as a working electrode. The counter electrode was made of a platinum mesh. The reference electrode was Ag/AgCl/KCl (sat.) with a Luggin probe positioned near the electrode surface. Linear sweep voltammograms were recorded by scanning the potential of the working electrode at a scan rate of 10 mV s^{-1} in 1 M KOH solution. The potential throughout the work was measured against the Ag/AgCl/KCl (sat.), then was converted to the normal hydrogen electrode (NHE) by adding 0.197 V.

3. RESULTS AND DISCUSSION

3.1 Synthesis and characterization of porphyrins.

The free base porphyrin namely 5,10,15,20 tetrakis (5-bromothiophen-2-yl) porphyrin (**1a**) was prepared following a modified literature procedure [46] by condensation of 5-bromothiophene-2-carbaldehyde (**2**) and pyrrole (**3**) at 140 ^{o}C under argon atmosphere using *p*-toluene sulphonic acid as a catalyst and DMF as a solvent. After purification by column chromatography and crystallization, the free base porphyrin (**1a**) was obtained as dark violet crystals in 55% yield (Scheme 1). The metalloporphyrins (cobalt and copper, **1b** and **1c** respectively scheme 1) were obtained in almost quantitative yield by heating the free base porphyrin (**1a**) with excess of metal acetate (MAc) of either cobalt or copper in DMF at 100 ^{o}C for one hour (Scheme 1).

The chemical structure of the porphyrins (**1a-c**) was confirmed by spectroscopic techniques (IR, NMR, MS, and UV-Vis.) and compared with the previously reported data [46].

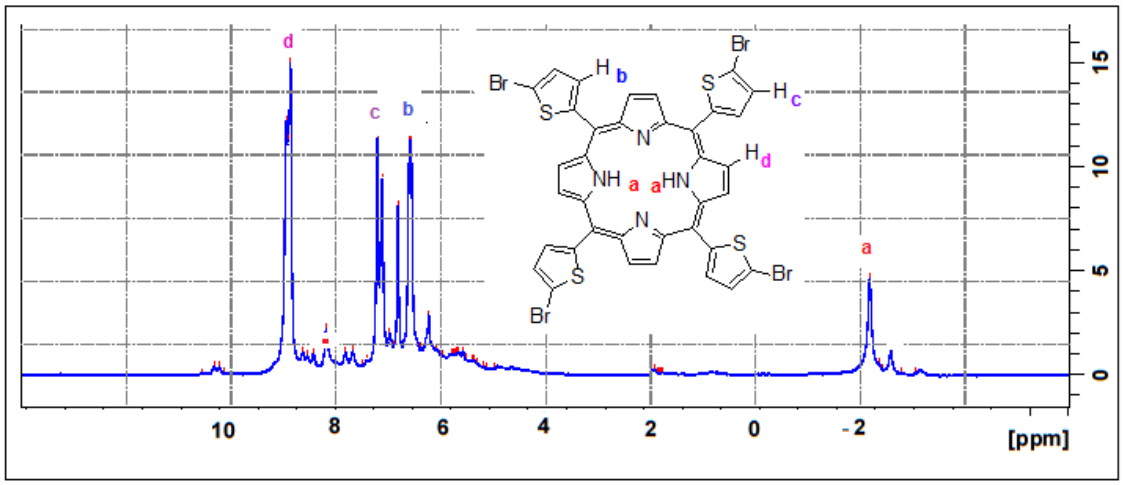

Figure 1. ^{1}H-NMR spectrum of the free base porphyrin (**1a**) in $CDCl_3$.

The ^{1}H-NMR spectrum of the free-base porphyrin (**1a**) (figure 1) revealed a singlet signal at a very up-field value and appeared at -2.52 ppm attributed to the characteristic inner protons of the porphyrin ring (2NH). Additionally, a downfield multiplet at 9.23 ppm recognized to the *beta* hydrogens of the porphyrin ring system. Also, two different multiplets at 6.56 and 7.42 ppm accredited to the H-3 and H-4 of the thiophene rings respectively. On the other hand, the ^{1}H-NMR spectra of the metalloporphyrins (**1b, c**) are similar to the spectrum shown in figure 1, apart from the disappearance of the N-H signal at -2.52 ppm which is due to the replacement of the two inner porphyrin hydrogens by the metal ion (cobalt or copper) to form metalloporphyrins (**1b, c**) respectively. Furthermore, the FT-IR spectra (Figure 2) of both the cobalt and copper metalloporphyrins (**1b,c**) revealed the disappearance of all mode of vibrations of the inner N-H bonds. Therefore, in the FT-IR spectra, the free-base porphyrin **(1a)**, revealed peaks at 3415, 1598 and 950 cm^{-1} which can be attributed to the in-phase stretching, in-plane deformation and the out-plane deformation vibration modes of the N-H

bonds [47]. Also, all the investigated porphyrins showed a very weak peak at 3110 cm^{-1} attributed to the stretching vibration mode of the C-H bonds of the aromatic ring systems .

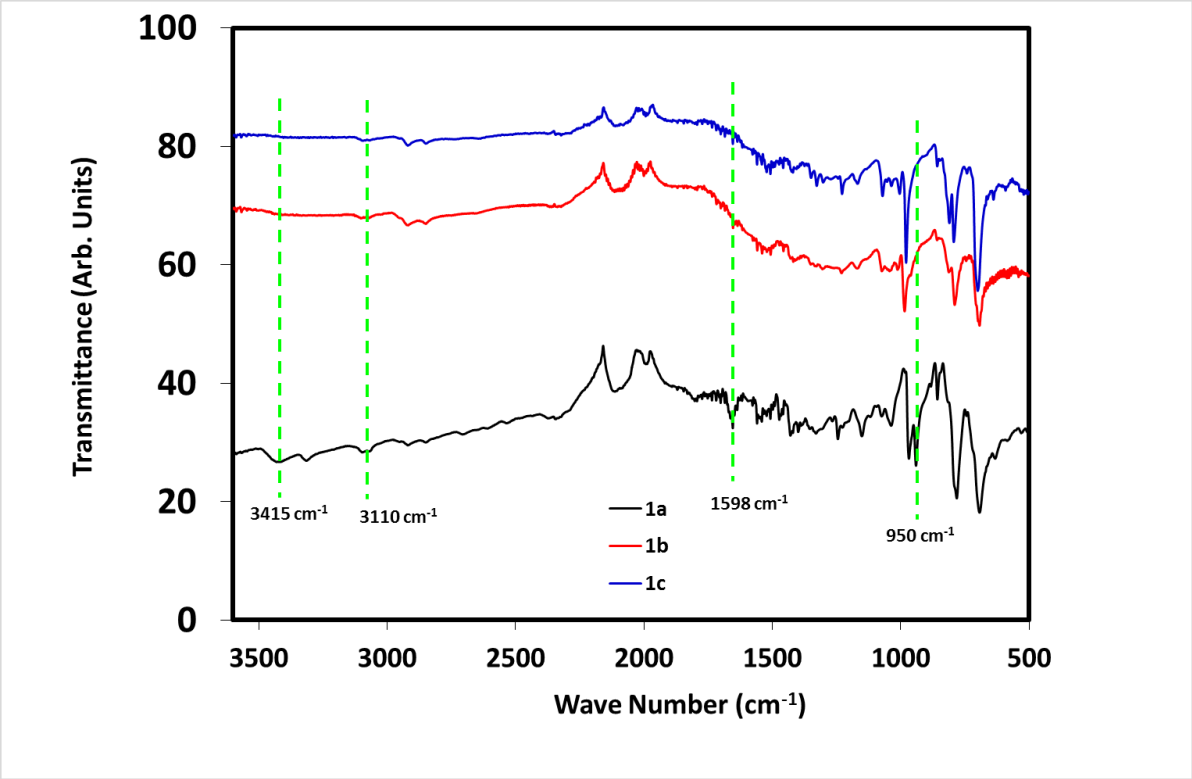

Figure 2. FT-IR Spectra of the free-base porphyrin **(1a)** and the cobalt and copper metalloporphyrins (**1b, 1c**) The dashed lines at 3415, 3415, 1598 and 950 cm^{-1} indicate the position of the N-H bands, also the band at 3110 cm^{-1} is attributed to the stretching vibration mode of the C-H bonds of the aromatic ring systems.

3.2 UV-Vis absorption and band gap measuring

The UV-Vis absorption spectra and the extracted data for both free-base porphyrin (**1a**), cobalt-porphyrin (**1b**) and copper-porphyrin (**1c**) are shown in figure 3 and table1, respectively. The free-base porphyrin (**1a**) and metalloporphyrins (**1b, c**) revealed very strong Soret bands at 430, 419 and 423 nm, respectively. The free-base porphyrin (**1a**) showed a typical *etio*-porphyrin Q bands pattern and appeared at 522, 566, 600 and 660 nm [4]. While, the cobalt and copper porphyrins showed one band each at 537 and 548 nm for (**1b**) and (**1c**), respectively.

The band gap energy was calculated from the UV-Vis absorption spectra shown in figure 3, using equation 1 [48]. The calculated values are reported in table 1:

$$E = h\,C/\lambda \qquad (1)$$

Where E is the band gap energy, h = Plank's constant (6.626 x 10^{-34} Joule sec), C = speed of light (3.0 x 10^{8} meter/sec) and λ is the cut-off wavelength of the Soret bands (when the absorption value is minimum).

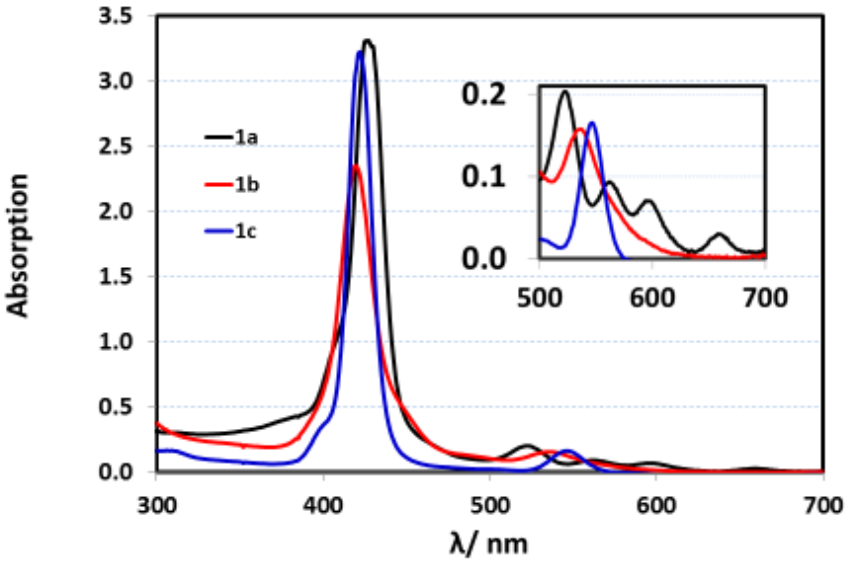

Figure 3. UV-Vis absorption spectra in CH_2Cl_2 for the free-base porphyrin (**1a)**, cobalt porphyrin (**1b**) and copper porphyrin **(1c)**. The inset shows a magnified view of the Q bands region.

It is worthy to mention that, the insertion of the metal ion inside the porphyrin molecule (**1a)** *via* forming new bonds with the two diagonal nitrogen atoms; causes a slight blue shift for both Soret and Q bands of the free-base porphyrin. These results are in agreement with previously reported studies, which indicated the existence of a slight distortion in the porphyrin ring planarity when a metal ion was introduced inside the porphyrin ring [49-50].

Table 1. UV-Vis Absorption data and the calculated band gap of the free-base porphyrin (**1a)**, cobalt porphyrin (**1b**) and copper porphyrin **(1c)**.

Porphyrin	Absorption (A)	Wavelength λ (nm)	Log ε	Band gap (eV)*
1a	2.752, 0.198, 0.101, 0.082, 0.035	430, 522, 566, 600, 660	4.20, 3.37, 3.08, 2.99, 2.60	2.74
1b	3.052, 0.293	419, 537	4.33, 3.44	2.68
1c	3.282, 0.248	423, 548	4.30, 3.44	2.81

*Where 1ev = 1.6 x 10^{-19} Joules

3.3 The thermal gravimetric analysis (TGA)

The thermal gravimetric analyses (TGA) were performed using a TGA instrument (TA Instruments - Q50), under a Nitrogen atmosphere with a heating rate of 10 °C/min, from 25 to 700°C. The TGA curves for the free-base porphyrin (**1a**) and metalloporphyrins (**1b**) and (**1c**) are shown in figure 4.

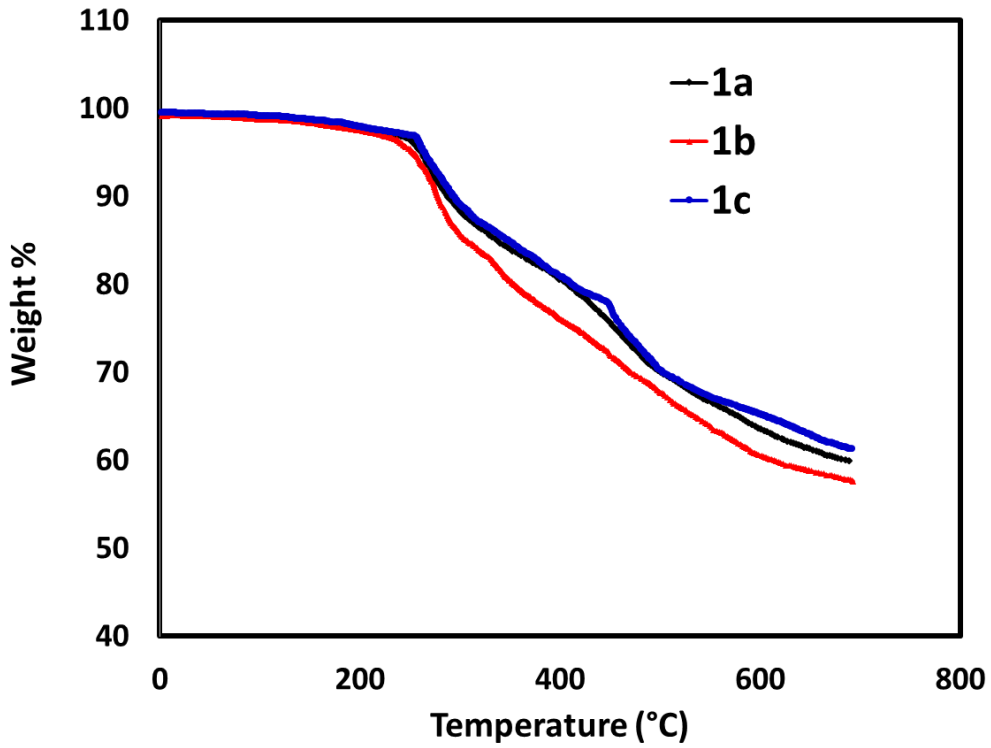

Figure 4. TGA Curves for porphyrin (**1a**), metalloporphyrins (**1b**) and (**1c**). The curves were recorded for the samples under nitrogen atmosphere with a heating rate of 10 °C/min, from 25 to 700°C.

The thermal decomposition of the free-base porphyrin (**1a**) and metalloporphyrins (**1b, c)** takes place in two primary decomposition stages. The first stage, from 100 to 250°C, involves the decomposition of the physically adsorbed water. While, the second stage (from 250 to 700°C) includes the decomposition of porphyrin scaffold. The onset decomposition temperatures (T_{onset}), at which the investigated samples begin to disintegrate, are reported in table 2. The values of T_{onset} per each sample were extracted from TGA curves shown in figure 4.

Table 2. Measured T_{onset} temperatures for free-base porphyrin **(1a),** metalloporphyrins **(1b)** and **(1c).**

Decomposition	Free-base porphyrin **(1a**)	Co- porphyrin (**1b**)	Cu- porphyrin (**1c**)
T_{onset1}	141	141	141
T_{onset2}	270	280	270
Residual mass (%) at 700°C	57.6	57.6	61.3

The thermogravimetric analyses behavior of the three investigated porphyrins is relatively similar. The mass loss up to 250 °C is less than 1%. A significant mass loss was observed at a temperature higher than 250 °C for the three samples. The residual mass percent after 700 °C were 57.6, 57.6 and 61.3 % for the free-base porphyrin (**1a**), metalloporphyrin (**1b**) and **1c** respectively. The obtained results confirm that the three porphyrins are thermally stable up to 250 °C, and the insertion of the transition metals into the porphyrin ring system did not adversely affect their robustness.

3.4 Porphyrins electrocatalyst for oxygen evolution reaction (OER).

The splitting of water, equation 2, by electrolysis into oxygen and hydrogen is a promising technology in producing clean and sustainable energy. The water splitting process requires high energy. The process involves two half-reactions namely oxygen evolution reaction (OER) and hydrogen evolution reaction (HER). Equations 3 and 4 express the OER and HER reactions in 1 M acidic solution [51]:

$$2H_2O \rightarrow 2H_2 + O_2 \quad (2)$$

$$2H_2O \rightarrow O_2 + 4H^+ + 4\,e^- \quad (V_{anode} = 1.23 \text{ V vs Normal Hydrogen Electrode (NHE)}) \quad (3)$$

$$4H^+ + 4e^- \rightarrow 2\,H_2 \quad (V_{cathode} = 0.0 \text{ V vs Normal Hydrogen Electrode (NHE)}) \quad (4)$$

The OER is a four-electron and four-proton process and involves the formation of rigid O-O bond; therefore, the OER is the rate-determining step in the water-splitting technology [52-53]. Electrocatalytic activities of the free-base porphyrin (**1a**) cobalt-porphyrin (**1b)** and copper-porphyrin (**1c**) toward the OER were investigated in 1 M KOH solution. The porphyrin electrocatalyst was prepared by coating the surface of the Pt electrode with a layer of the required porphyrin. The porphyrin coated electrode was used as a working electrode during electrochemical measurements. Figure 5 shows linear sweep voltammograms (LSVs) obtained for a base Pt electrode and electrodes modified with porphyrins (**1a**), (**1b**) and (**1c**) respectively.

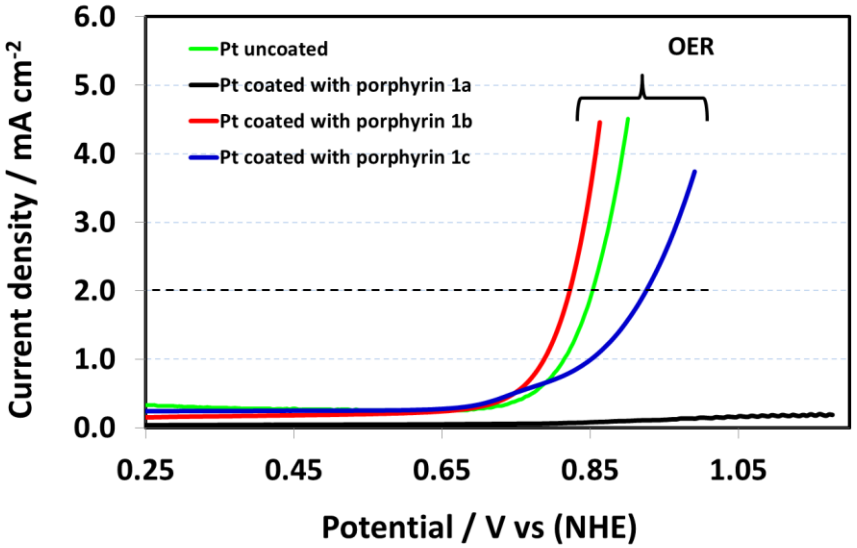

Figure 5. Linear sweep voltammograms recorded at uncoated Pt electrode and Pt electrodes coated with porphyrin **1a, 1b** and **1c** respectively. The scan rate was 10 mV s^{-1} in 1 M KOH solution. The dashed line indicates the electrode potential corresponds to a current density of 2 mA cm^{-2}. The braces symbol indicates the OER region.

The scan rate was 10 mV s^{-1}. The projected surface area of the base Pt electrode was used to calculate the current density in mA cm^{-2}. The performance of the electrocatalyst is evaluated by calculating the overpotential (η) in mV, which is the difference between the applied potential (E) and potential under equilibrium conditions (E_{eq}). Good catalysts perform oxygen evolution process and low η.

$$\eta = E - E^0 \quad (5)$$

The equilibrium potential for the OER in 1 M acidic solution is 1.23 V versus *NHE* . The potential of the reaction is pH dependent and can be expressed according to the Nernst equation 6 [54].

$$E^0_{\text{ in 1 M KOH}} = E^0_{\text{ in 1 M acidic solution}} - 0.059\ pH\ vs\ NHE \quad (6)$$

The equilibrium potential for the OER in 1 M KOH ($E^0_{\text{ in 1 M KOH}}$) was 0.404 V versus the *NHE*, this value was calculated from equation 6. The applied potential (E), corresponds to a current density of 2 mA cm^{-2}, were extracted from LSVs in figure 6 for the uncoated Pt electrode and coated electrodes with porphyrins (**1a**), (**1b**) and (**1c**), respectively. Then, the extracted applied potential E and equilibrium potential ($E^0_{\text{ in 1 M KOH}}$) were used to calculate η. The data are reported in table 3. Although, the Pt-coated with cobalt-porphyrin (**1b**) layer is expected to have less electric conductivity than the bare Pt electrode; it showed better electrocatalytic activity towards the OER than the bare Pt electrode.

Table 3. The overpotential (η) values correspond to a current density of 2 mA cm^{-2} calculated from the linear sweep voltammograms shown in figure 6 for uncoated Pt electrodes and Pt electrodes coated with porphyrins (**1a**)**,** (**1b**) and (**1c**).

Electrode	Overpotential *(η) in* mV VS NHE at a current density of 2 mA cm^{-2}
Pt uncoated	451
Pt-coated with **1a**	NA
Pt-coated with **1b**	419
Pt-coated with **1c**	523

The η value was 419 mV for cobalt-porphyrin (**1b**) which is lower than the value obtained for the bare Pt electrode (451 mV). The η value obtained for the copper-porphyrin (**1c**) (523 mV) was much higher than the base Pt electrode, indicating a poor electrocatalytic activity. The obtained results are in good agreement with what is reported in the literature regarding the excellent electrocatalytic activities of the cobalt porphyrin electrodes [55]. Table 4 compares the η value of the cobalt-porphyrin electrode with values reported in the literature for other organometallic based catalysts [53]. On the other hand, the activity of the free-base porphyrin (**1a**) was very poor, which confirms the crucial role of the central transition metal in enhancing the activities of the catalyst [55].

Table 4. Compares the OER overpotential (η) values obtained for the Pt electrode coated with porphyrins (**1a**)**,** (**1b**) and (**1c**) with values reported in the literature for other organometallic based catalysts.

Catalyst	Electrolyte Solution	Overpotential *(η) in* mV VS NHE	Current density mA/cm^2	Reference
Pt-coated with **1b**	0.1 M NaOH	419	2	
FeTpyp	0.1 M NaOH	480	0.5	45
CoTPyP	0.1 M NaOH	420	0.5	45

The stability of the cobalt-porphyrin catalyst was investigated by the chronoamperometry technique in 1 M KOH solution. The working electrode was a Pt-coated with porphyrin (**1b**), the potential of this electrode was stepped from an initial potential of 0 V to a final potential of 0.74 versus *NHE*. The ultimate potential, 0.74 V, was particularly selected to match the value, which is required to drive the OER at the electrode surface. The produced Faradaic current was recorded against time, as shown in figure 6. The fluctuation in current values, hence noisy curve, is due to the formation of oxygen gas bubbles from water splitting reaction. The gas bubbles were observed at the surface of the electrode during the experiment. Also, the observed increase in the current with time could be

attributed to the fact that more of the cobalt porphyrin catalyst become accessible with time. The electrode was able to maintain its activity for up to 30 min. After that, the coated layer begins to delaminate off the base electrode.

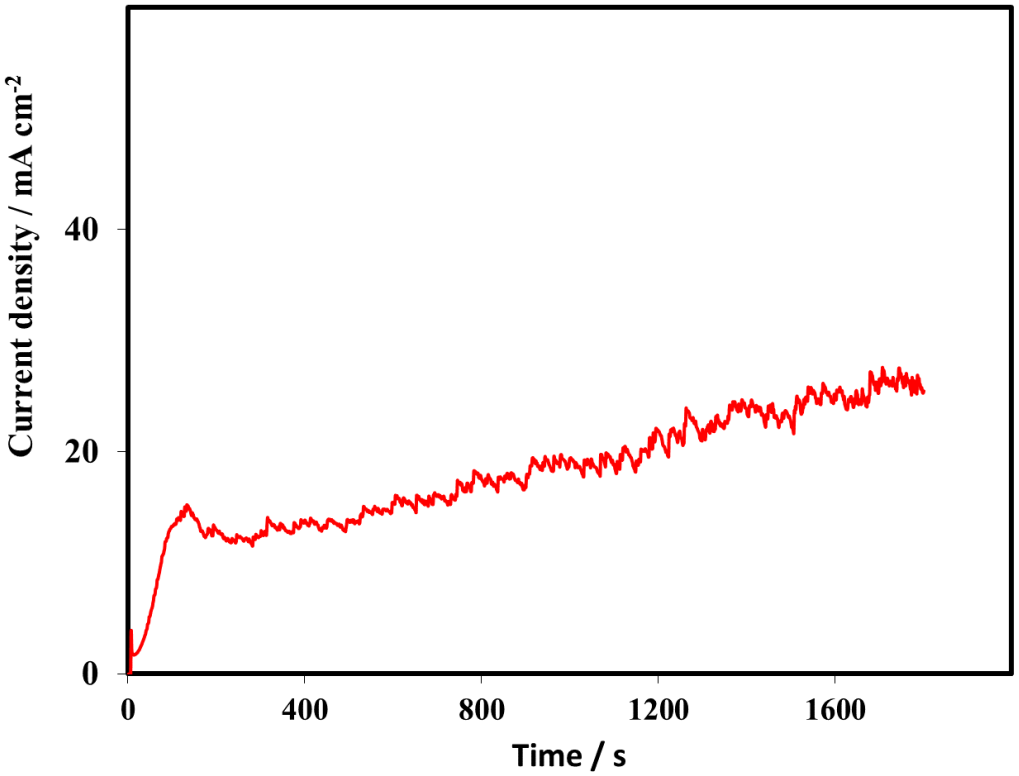

Figure 6. Current versus time curve recorded for Pt electrodes coated with cobalt porphyrin (**1b)** in 1 M KOH; the potential was stepped from 0 to 0.74 V versus NHE.

The enhanced catalytic activities of the cobalt porphyrin (**1b**) could be due to its low bandgap energy, i.e., cobalt-based porphyrin requires less energy than copper porphyrin to stabilize high-valent metal ions (metal-oxo units), which are generally believed to be involved as key intermediates in oxygen evolution catalytic cycles [43].

4. CONCLUSION

Free-base *meso*-tetrabromothiophenyl porphyrin (**1a**) and cobalt (**1b**) and copper (**1c**) complexes were prepared in a good yield following modified literature procedure. The data obtained from NMR, FT-IR, MS and UV-Vis confirmed the attachments of the four peripherals 5-bromothiophen-2-yl in the *meso* position of the porphyrin ring system. Also, the insertion of the transition metals to form metalloporphyrin complexes was proved by the absence of the NMR signals at -2.52 ppm and FT-IR peak at 3415 cm^{-1} and other vibration modes. The synthesized porphyrins showed very good thermal stability up to 250 °C. Additionally, the cobalt-porphyrin (**1b**) showed better catalytic activity toward the OER than the copper-porphyrin (**1c**) and the free-base porphyrin (**1a**). The values of the overpotential corresponding to a current of 2 mA cm^{-2} were 419 mV, 451 mV

and 523 mV for the cobalt porphyrin (**1b**) electrode, the uncoated Pt-electrode and the copper porphyrin (**1c**) electrode, respectively. Moreover, the (**1b**) electrode showed good stability as a catalyst for the OER and maintained producing O_2 at a current density more than 10 mA cm^{-2} for 30 min.

ACKNOWLEDGEMENTS
The authors are grateful to the Deanship of Scientific Research at King Faisal University for the financial support (project number 170042).

References

1. G. C.Ferreira, handbook of porphyrin science : with applications to chemistry, physics, materials science, engineering, biology and medicine, World Scientific Pub. Co, USA (2014).
2. L. P. Cook, G. Brewer, W. Wong-Ng, *Crystals*, 7 (2017) 223.
3. I. Elghamry, L. F. Tietze, *Tetrahedron Lett*., 49 (2008) 3972.
4. R. Giovannetti, Macro To Nano Spectroscopy**,** InTech, London (2012)**.**
5. M. M. El-Nahass, A. A. M. Farag, M. El-Metwally, F. S. H. Abu-Samaha, E. Elesh, *Synth. Met.,* 195 (2014) 110.
6. S. F. Pop, R. M. Ion, *Proc. SPIE* 8411, Advanced Topics in Optoelectronics, Microelectronics, and Nanotechnologies VI (2012) 84111L.
7. Q. H. Al-Galiby, H. Sadeghi, L. A. Algharagholy, I. Grace, *Nanoscale,* 8 (2016) 2428.
8. S. Nadeem, F. Iqbal, M. Ibrahim, A. Mutalib, B. Abdullah, M. S. Shaharun, *AIP Conf. Proc.,* (2017) 1891.
9. A. Gupta, L. N. Goswami, M. Ethirajan, J. Missert, K. V. K. Rao, *J. Porphyr. Phthalocyanines* , 15 (2011) 401.
10. R. K. Pandey, S. Constantine, D. A. Goff, A. N. Kozyrev, T. J. Dougherty, K. M. Smith, *Med. Chem. Lett*., 6 (1996) 105.
11. K. S. Suslick, N. A. Rakow, M. E. Kosal*, J. Porphyr. Phthalocyanines,* 4 (2000) 407.
12. C. M. B. Carvalho, T. J. Brocksom, K. T. de Oliveira, *Chem. Soc. Rev*., 42 (2013) 3302.
13. S. Pisarek, K. Maximova, D. Gryko, *Tetrahedron*, 70 (2014) 6685.
14. D. Wang, J. T. Groves, *Proc. Natl. Acad. Sci*., 110 (2013) 15579.
15. E. S. Da Silva, N. M. M. Moura, M. G. P. M. S. Neves, A. Coutinho, M. Prieto, C. G. Silva, J. L. Faria, *Appl. Catal. B Environ*., 221 (2018) 56.
16. C. Costentin, S. Drouet, M. Robert, J. M. Saveant, *Science*, 338 **(**2012) 90.
17. M. D. Kärkäs, B. Åkermark, *Dalt. Trans.,* 45 (2016) 14421.
18. D. Quezada, J. Honores, M. Garcí, F. Armijo, M. Isaacs, *New J. Chem*., 8 (2014) 3606.
19. J. Jiang, K. L. Materna, S. Hedström, K. R. Yang, R. H. Crabtree, V. S. Batista, G. W. Brudvig, *Angew. Chemie - Int. Ed*., 129 (2017) 9239.
20. S. Swavey, D. Fresh, *Am. J. Anal. Chem.,* 4 (2013) 54.
21. J. Shen, R. Kortlever, R. Kas, Y. Y. Birdja, O. Diaz-Morales, Y. Kwon, I. Ledezma-Yanez, K. J. P. Schouten, G. Mul, M. T. M. Koper, *Nat. Commun*., 6 (2015) 8177.
22. M. C. Gallo, B. M. Pires, K. C. F. Toledo, S. A. V. Jannuzzi, E. G. R. Arruda, A. L. B. Formiga, J. A. Bonacin, *Synth. Met.,* 198 (2014) 335.
23. P. Muthukumar, S. Abraham John, *J. Colloid Interface Sci.,* 421 (2014) 78.
24. C. Z. Li, S. Alwarappan, W. Zhang, N. Scafa, X. Zhang, C. Li, *Am. J. Biomed. Sci.,* 1 (2009) 274.
25. P. D. Beer, M. G. B. Drew, R. Jagessar, S. *J. Chem. Soc. Dalt. Trans*., (1997) 881.
26. S. Chandra, C. Mende, D. Bahadur, A. Hildebrandt, H. Lang, *J. Solid State Electrochem*., 19 (2014) 169.
27. M. Biesaga, K. Pyrzyńska, M. Trojanowicz, *Talanta,* 51 (2000) 209.

28. G. Zuo, X. Liu, J. Yang, X. Li, X. Lu, *J. Electroanal. Chem.,* 605 (2007) 81.
29. S. S. Ishihara, S. Ishihara, J. Labuta, W. Van Rossom, D. Ishikawa, K. Minami, J. P. Hill, K. Ariga, *PCCP,* 16 (2014) 9713.
30. T. Higashino, H. Imahori*, Dalt. Trans.,* 44 (2015) 448.
31. J. X. Zhang, F. M. Han, J. C. Liu, R. Z. Li, N. Z. Jin, *Tetrahedron Lett*., 57 (2016) 1867.
32. 32. S. Choi, B. I. Sang, J. Hong, K. J. Yoon, J. W. Son, J. H. Lee, B. K. Kim, H. *Kim*, *Sci. Rep.,* 7 (2017) 41207.
33. N. Jiang, T. Sumitomo, T. Lee, A. Pellaroque, O. Bellon, D. Milliken, H. Desilvestro, *Sol. Energy Mater. Sol. Cells*., 119 (2013) 36.
34. B. Momo, P. Pavani, C. Baptista, M. Brocksom, T. Thiago, K. De Oliveira, *Eur. J. Org. Chem.,* (2014) 4536.
35. A. D. Alder, F. R. Longo, J. D. Finarelli, J. Goldmacher, J. Assour, L. Korsakoff, *J. Org. Chem*., 32 (1967) 476.
36. A. Fidalgo-Marijuan, G. Barandi, M. Urtiagaa, I. Arriortua, *Cryst. Eng. Comm***.,** 15 (2013) 4181.
37. Z. Xiaoyuan, Z. Biaobiao, Z. Li, L. Ping, D. Wenji**,** *Synth. Commn.,* 45 (2013) 2730.
38. X. Wei, X. Du, D. Chen, Z. Chen, *Thermochim. Acta*, 440 (2006) 181.
39. N. M. Berezinam D. N. Minh, Y. I. Tikhonova, N. N. Tumanova, S. S. Guseinov, M. I. Bazanov, M. B. Berezin, A. V. Glazunov, A. S. Semeikin, *Russian Journal.of General Chemistry,* 186 (2016) 835.
40. A.Uygun, O. Turkoglu, S. S. Ersoy, A. Yavuz, G. G. Batir, *Curr. Appl. Phys*.**,** 9 (2009) 866.
41. F. Igor. Perepichka, D. F. Perepichka, Handbook of Thiophene-Based Materials: Applications in Organic Electronics and Photonics, Wiley-VCH, Weinheim (2009).
42. C. H. Lee, D. K. Dogutan, D. G. Nocera, *J. Am. Chem. Soc*., 133 (2011) 8775.
43. Y. Han, H. Fang, H. Jing, H. Sun, H. Lei, W. Lai., R. Cao, *Angew. Chemie - Int. Ed,* 55 (2016) 457.
44. J. E. Pander, A. Fogg, A. B. Bocarsly, *Chem. Cat. Chem.,* 8 (2016) 3536.
45. B. Wurster, D. Grumelli, D. Hotger, R. Gutzler, K. Kern, *J. Am. Chem. Soc.,* 138 (2016) 3623.
46. R. Prasat; P. Bhavana, *J. Heterocyclic Chem.,*49 (2012) 1044.
47. P. Şen, C. Hirel, C. Andraud, C. Aronica, Y. Bretonnière, A. Mohammed, H. Ågren, B. Minaev, V. Minaeva, G. Baryshnikov, H. Hsun Lee, J. Duboisset, M. Lindgren, *Material,* 3 (2010) 4446.
48. J. Dharma, A. Pisal, PerkinElmer, *Inc. Application note: UV/Vis/NIR spectrometer* (2009).
49. Z. Valicsek, O. Horváth, *Microchem. J.,* 107 (2013) 47.
50. A. Hoshino, Y. Ohgo, M. Nakamura, *Tetrahedron Lett*., 46 (2005) 4961.
51. A. V. Meier, Electric power systems: a conceptual introduction, Wiley-VCH, Weinheim (2006).
52. C. McCrory, S. Jung, I. Ferrer, S. Chatman, J. Peters, T. Jaramillo, *J. Am. Chem. Soc.,* 137 (2015) 4347.
53. N. Suen, S. Hung, Q. Quan, N. Zhang, Y Chen. Xu, *Chem. Soc. Rev*., 46 (2017) 337.
54. A. J. Bard, L. R. Faulkner, Electrochemical Method, Wiley-VCH, Weinheim (2000).
55. A. Han, H. Jia, H. Ma., S. Ye, H. Wu, H. Lei, Y. Han, R. Cao, P. Du, *PCCP,* 16 (2014) 11209.